Interfacial benzenethiol modification facilitates charge transfer and improves stability of cm-sized metal halide perovskite solar cells with up to 20 % efficiency

Journal:	*Energy & Environmental Science*
Manuscript ID	EE-ART-03-2018-000754.R2
Article Type:	Paper
Date Submitted by the Author:	19-Apr-2018

Complete List of Authors:	Lu, Jian-Feng; Monash University, School of Chemistry Lin, Xiongfeng; Monash University, Department of Materials Science and Engineering Jiao, Xuechen ; Monash University, Department of Materials Science and Engineering Gengenbach, Thomas; CSIRO, Materials Science and Engineering Scully, Andrew; Australian Commonwealth Scientific and Research Organization, Material Science and Engineering Jiang, Liangcong; Monash University, Department of Materials Science and Engineering Tan, Boer ; Monash University, Department of Materials Science and Engineering Sun, Jingsong ; Monash University, Department of Materials Science and Engineering Li, Bin; Monash University, Department of Materials Science and Engineering Pai, Narendra; Monash University, School of Chemistry bach, udo; Monash University, Department of Chemical Engineering Simonov, Alexandr; Monash University, School of Chemistry Cheng, Yi-Bing; Monash University, Materials Engineering

Interfacial benzenethiol modification facilitates charge transfer and improves stability of cm-sized metal halide perovskite solar cells with up to 20 % efficiency

Jianfeng Lu,[a] Xiongfeng Lin,[b] Xuechen Jiao,[c] Thomas Gengenbach,[d] Andrew D. Scully,[d] Liangcong Jiang,[c] Boer Tan,[c] Jinsong Sun,[c] Bin Li,[c] Narendra K. Pai,[a] Udo Bach,[b,d,e] Alexandr N. Simonov,[*a,f] Yi-Bing Cheng[c,e,g]

Broader context

Photovoltaic technology offers a sustainable solution to soaring global energy demands. The domination of crystalline silicon solar cells is expected to ease in the foreseeable future as they approach their theoretical efficiency limit. Metal-halide perovskite solar cells have emerged as the fastest-developing new photovoltaic technology rivalling crystalline silicon, largely due to its compatibility with large-scale production using conventional printing processes. The transition from research to industrial applications of perovskite solar cells requires further advancements in both operational stability and large-area device fabrication; two factors that often display an inverse inter-dependency. The present work demonstrates that incorporation of certain benzenethiol derivatives at the interface between the perovskite light absorber layer and the layer of hole-transporting material provides the dual benefit of improvement in the band-energy alignment and also protection of the perovskite from environmental degradation. A key feature of this work is the use of cm-sized devices rather than the mm-scale solar cells commonly employed for research purposes. The simple approach developed here enables fabrication of larger cells with characteristics that are very similar to those of smaller devices.

Journal Name

ARTICLE

Interfacial benzenethiol modification facilitates charge transfer and improves stability of cm-sized metal halide perovskite solar cells with up to 20 % efficiency

Received 00th January 20xx,
Accepted 00th January 20xx

DOI: 10.1039/x0xx00000x

www.rsc.org/

Jianfeng Lu,[a] Xiongfeng Lin,[b] Xuechen Jiao,[c] Thomas Gengenbach,[d] Andrew D. Scully,[d] Liangcong Jiang,[c] Boer Tan,[c] Jinsong Sun,[c] Bin Li,[c] Narendra K. Pai,[a] Udo Bach,[b,d,e] Alexandr N. Simonov,[*a,f] Yi-Bing Cheng[c,e,g]

Metal halide perovskite solar cells (PSC) exhibit outstanding power conversions efficiencies when fabricated as mm-sized devices, but creation of high-performing large-area PSCs that are stable under operating conditions on a sufficiently long timescale still presents a significant challenge. We demonstrate herein that modification of the interface between the perovskite and spiro-OMeTAD hole-transporting material with commercially available *para*-substituted benzenethiol molecules facilitates fabrication of cm-sized PSCs with both improved efficiency and stability. Comprehensive analysis using specialised and conventional physical characterisation techniques has been undertaken to demonstrate that band alignment at the perovskite surface can be tuned to improve the solar cell efficiency *via* adsorption of benzenethiols with a significant dipole moment. Moreover, modification of the perovskite with cyano-substituted benzenethiol enhances charge extraction and reduces charge recombination in the devices. These effects enable improvements in the power conversion efficiency of PSCs from 19.0 to 20.2 % and from 18.5 to 19.6 % under 1 sun AM 1.5G irradiation with 0.16 and 1.00 cm^2 aperture, respectively. Most importantly, benzenethiol-modified perovskite solar cells retain more than 80 % of the initial performance after 185 h of continuous operation at 50 % relative humidity and 50 °C device temperature under 1 sun irradiation, while devices with no interfacial modification undergo continuous deterioration down to 35 % of the initial efficiency. These significant improvements are provided by a very simple and perfectly reproducibile modification procedure that can be readily adopted in other types of PSCs.

Introduction

New breakthroughs in photovoltaic technology are urgently needed to promote the global transition to solar power as a major, essentially inexhaustible source of energy. Although silicon-based photovoltaic technology that dominates the existing solar cell market has proven to be highly reliable, further improvements in their intrinsic efficiency are not straightforward.[1] Instead, so-called 3rd generation solar cells have come to the forefront of photovoltaic research and have seen unprecedented progress recently.[2] For example, metal halide perovskite solar cells (PSCs) technology has now reached an outstanding certified power conversion efficiency (PCE) of 22.7% after only eight years of active investigations.[3] This has been achieved *via* numerous improvements and optimisations of the perovskite light-absorber composition,[4-6] deposition procedures,[7-9] selective charge transporting materials,[10, 11] and interface engineering.[12-14] Many of these methods were developed not only to improve the efficiency but also to address a major weakness of the metal halide perovskites, *viz.* instability under operating conditions.[15]

In a typical PSC, a light-absorber is confined between layers of electron-selective and hole-selective transporting materials (ETM and HTM, respectively). Diffusion lengths of photo-generated charge carriers in metal halide perovskites are on the micrometer scale under solar illumination, and hence transport losses within these materials are very low.[16] Thus, major losses occur due to recombination across the perovskite|ETM and perovskite|HTM interfaces. The properties of these interfacial regions determine both the initial photovoltaic performance and stability of the solar cells, as documented in a plethora of recent publications focusing on optimisation of interfaces in PSCs.[17, 18] For example, it was reported that ionic defects at the surfaces and grain boundaries of perovskite films are detrimental to both the

[a] School of Chemistry, Monash University, Victoria, 3800, Australia
E-mail: alexandr.simonov@monash.edu
[b] Department of Chemical Engineering, Monash University, Victoria 3800, Australia
[c] Department of Materials Science and Engineering, Monash University, Victoria, 3800, Australia
[d] CSIRO manufacturing, Clayton, Victoria 3168, Australia
[e] ARC Centre of Excellence for Exciton Science, Monash University, Victoria, 3800, Australia
[f] ARC Centre of Excellence for Electromaterials Science, Monash University, Victoria, 3800, Australia
[g] State Key Laboratory of Advanced Technology for Materials Synthesis and Processing, Wuhan University of Technology, Wuhan 430070, China

Electronic Supplementary Information (ESI) available: experimental section; XRD, SEM, AFM, FTIR, XPS, UPS, KPFM, photo/electroluminescence, and photovoltaic data. See DOI: 10.1039/x0xx00000x

efficiency and stability of PSCs.[19, 20] Snaith and co-workers found that iodopentafluorobenzene and Lewis bases, such as pyridine or thiophene, efficiently passivate trap states on the perovskite surface *via* interaction with the under-coordinated halide anions and metal cations that act as charge-carrier recombination centers.[17] Yang and Huang demonstrated that a layer of quaternary alkyl ammonium cations on the perovskite surface can substantially reduce the charge trap density and elongate the charge carrier lifetime, improving both device performance and stability.[21, 22] More recently, Seok and colleagues reported that additional iodide ions in the organic cation solution decreases the concentration of deep-level defects in perovskite films. This rational defect-engineering of the perovskite layer resulted in the highest PCE for PSCs reported to date.[3]

It has also been reported that the electric field at a typical perovskite|HTM or ETM|perovskite interface is not strong enough to sustain efficient electron or hole extraction.[23-25] Accumulation of electrons and holes at the perovskite surface and subsurface close to the interface is currently considered to be responsible for the performance hysteresis behaviour and irreversible degradation of PSCs.[18] Several groups reported that the problem can be mitigated *via* introduction of specifically designed interlayers between perovskite and a charge-selective material, which can additionally stabilise devices *via* surface passivation.[26] For example, a π-conjugated Lewis base with *n*-type semiconductor property 1,1-dicyanomethylene-3-indanone was used to promote charge extraction at the interface between methyl ammonium lead iodide and ETM, while also improving the stability *via* scavenging Lewis acid traps on the surface and at the grain boundaries of the perovskite.[27] In another report, a strong interfacial dipole moment was created between a perovskite light-absorber and C60 electron transporter by depositing a sub-nm layer of tris(2,4,6-trimethyl-3-(pyridin-3-yl)phenyl) borane to facilitate a fast charge sweep-out and suppress carrier recombination at the interface.[28] However, we are not aware of any previous reports on modification of the perovskite|HTM interfaces with dipoles to improve charge-transfer as it was done previously at the perovskite|ETM interfaces.

Most of the interface modification and other strategies devised hitherto with the aim to endow perovskite solar cells with high power conversion efficiencies and robustness were applied to devices of small active areas (~ 0.1 cm^2), whereas examples of larger high-performing perovskite solar cell are rare.[29-32] However, the performance of these small PSCs has now reached the level where demonstration of methods for fabrication of high-efficiency and stably operating cm-sized solar cells is an equally important and pressing scientific task.[2] Besides, creation of high-quality interfaces to prevent recombination and degradation becomes increasingly challenging with an increase in the active area of a device.[33-35] The present work explores the possibility for modification of the high-performing perovskite crystal surface with *para*-substituted benzenethiol molecules having different dipole moments. Such treatment was anticipated to modulate the band alignment at the perovskite|HTM interfaces, which could assist charge extraction and suppress carrier recombination. Furthermore, facilitated charge extraction can reduce the charge accumulation at the perovskite surface and thereby improve the lifetime of solar cells.[18]

Results and discussion

Solar cell architecture

All solar cells investigated in this work had a standard *n-i-p* architecture (**Figure 1a**) and were fabricated by sequential deposition of components onto a glass covered with fluorine-doped tin(IV) oxide, which served as an anode in the final device. Thoroughly optimised procedures adopted from literature[36] and established in our laboratory[6] were employed. The examined solar cells featured a *ca* 150 nm mesoporous titania scaffold (30 nm particle size) impregnated with a high-performing $Cs_{0.05}FA_{0.79}MA_{0.16}PbI_{2.49}Br_{0.51}$ perovskite (FA^+ = $CH(NH_2)_2^+$, MA^+ = $CH_3NH_3^+$) followed by *ca* 500 nm thick pure light-absorber, spiro-OMeTAD hole-selective layer and a gold counter electrode. TiO_2 and spiro-OMeTAD, which are the most widely employed electron- and hole-transporting materials in PSCs research, were employed here to facilitate comparisons of our results with the ample literature. A cross-sectional scanning electron microscopic (SEM) image of a typical PSC is exemplified in **Figure 1b**. The mixed perovskite was deposited by a one-step anti-solvent procedure followed by annealing at 100 °C for 60 min in an inert environment;[49] formation of the target material was confirmed by X-ray diffraction (XRD) analysis (**Figure S1**). XRD patterns exhibited a set of sharp reflections expected for the cubic $Cs_{0.05}FA_{0.79}MA_{0.16}PbI_{2.49}Br_{0.51}$ perovskite phase with a mean crystallite size of 142 ± 4 nm (derived from the full width at half maximum of the (100) peak). Weak diffraction peaks at 11° and 12.6° are associated with minor admixtures of yellow hexagonal δ_H phase and PbI_2.[5]

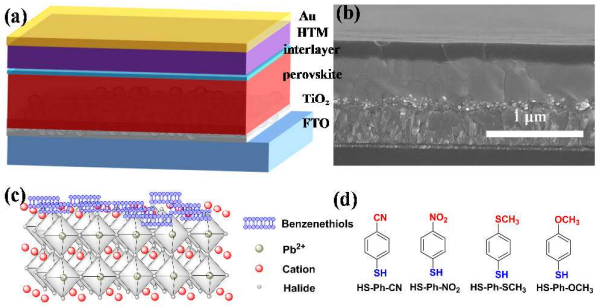

Figure 1. (a) Schematic presentation and (b) a typical cross-sectional SEM image of the investigated solar cells featuring a glass support covered with fluorine-doped tin(IV) oxide (FTO), compact TiO_2 coating (c-TiO_2), mesoporous TiO_2 substrate filled with the $Cs_{0.05}FA_{0.79}MA_{0.16}PbI_{2.49}Br_{0.51}$ perovskite (FA^+ = $CH(NH_2)_2^+$, MA^+ = $CH_3NH_3^+$), perovskite layer, interface modification, hole-transporting material spiro-OMeTAD and Au counter electrode. (c) Possible binding mode of a benzenethiol molecule on perovskite surface. (d) Chemical structures of benzenethiols used to modify the perovskite|HTM interface.

Adsorption of benzenethiols onto perovskite layer

According to the hard/soft acid/base theory, sulphur is a relatively soft (polarisable) atom. This defines the propensity of benzenethiols to bind to other soft elements/ions, in particular lead, which motivated us to use molecules featuring this functional group for interfacial modification of the perovskite surface. Among other possibilities, we chose benzenethiols as they can form rigid and dense hydrophobic layers. Moreover, *para*-substitution in the aromatic moiety allows for tuning the dipole moment of these molecules. Thus, benzenethiol derivatives *para*-substituted with –CN, $–NO_2$, $–SCH_3$, or $–OCH_3$ (**Figure 1d**) were examined. In some experiments, effects of modification of the perovskite layer with HS-Ph-F having significantly lower dipole moment were also studied.[37] Importantly, direction of molecular dipoles for HS-Ph-NO_2 and HS-Ph-CN is opposite to that for benzenethiols functionalised with –F, $–SCH_3$ and $–OCH_3$.[37]

Modification of the perovskite|HTM interface was achieved by spin-coating a 20 mM benzenethiol solution in chlorobenzene onto freshly deposited light-absorber layer prior to coating with a hole transporter. The morphology of the perovskite layer after surface treatment was examined by atomic force and scanning electron microscopy, showing no significant change as compared to the unmodified sample (**Figure S2**). A clear-cut confirmation of successful deposition of benzenethiols was derived from the XPS experiments undertaken using synchrotron radiation with photon energy of 488 eV (**Figure 2a**). Incident X-ray energy close to sulphur absorption edge significantly amplifies the photoelectron signal and thus the sensitivity of measurements.[38] More specifically, the intensity is enhanced approximately 10-fold as compared to the analysis carried out with 1486.7 eV photons. S $2p_{3/2}$ peaks within the binding energy range 164-165 eV manifesting in the spectra recorded for the benzenethiol-treated films were confidently attributed to thiol functionality.[39] Importantly, no sulphur could be detected with the unmodified sample even with this highly sensitive technique (**Figure 2a**). The Pb 4f spectra (recorded with conventional laboratory-based XPS instrument; **Figure S3**) of unmodified and HS-Ph-CN modified perovskite films exhibited one major doublet with the Pb $4f_{7/2}$ maximum at 138.4 eV, which is consistent with the Pb^{2+} oxidation state. Interestingly, a very weak signal with the Pb $4f_{7/2}$ peak at *ca*. 136.6 eV, which formally corresponds to Pb^0 state, was identified in the unmodified $Cs_{0.05}FA_{0.79}MA_{0.16}PbI_{2.49}Br_{0.51}$ perovskite, but not in the benzenethiol-treated sample. Unambiguous detection of an increase in the intensity at 137.8 eV due to formation of the Pb-S bonds upon modification with HS-Ph-CN was not successful due to very low amounts of introduced thiol. Both synchrotron-radiation and lab-based XPS also confirmed successful embedding of caesium into the perovskite structure (**Figure 2b**). Independence of the Cs 3d signal intensity on the presence of benzenethiols indicates that the latter are deposited as a very thin or even mono layer. This is also supported by FTIR and UV-Vis analysis, which were unable to unambiguously detect the benzenethiol-modification of perovskite surface under the employed conditions (**Figure S4**).

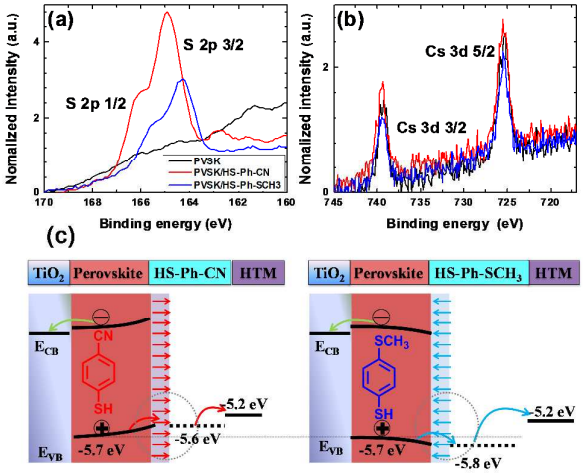

Figure 2. (a) S 2p and (b) Cs 3d spectra of the $Cs_{0.05}FA_{0.79}MA_{0.16}PbI_{2.49}Br_{0.51}$ perovskite films that were unmodified, or treated with either HS-Ph-CN or HS-Ph-SCH_3; data were derived from the synchrotron XPS analysis. (c) Hypothesised alteration of the energy levels at the perovskite|HTM interface under open-circuit conditions induced by modification with dipole benzenethiols. Valence band energy levels were derived from UPS experiments.

Impact of adsorbed benzenethiols on the electronic properties of the perovskite layer was probed by ultraviolet photoelectron spectroscopy (UPS). Ionisation potential was calculated as a difference between work function and highest occupied molecular orbital energy cut-off (**Figure S5**) and was assumed to be equal to the valence band energy level (E_{vb}). Unmodified $Cs_{0.05}FA_{0.79}MA_{0.16}PbI_{2.49}Br_{0.51}$ perovskite films exhibited E_{vb} of -5.7 eV, which is consistent with the value reported in literature.[40] Adsorption of benzenethiols induced small but detectable changes in the measured valence band energy level that were consistent with the direction of respective dipole moment of the examined molecules (**Figure 2c** and **Table S1**). However, the accuracy of this analysis is at the level of ± 0.1 eV, and therefore the detected band shifts should not be considered as an unambiguous proof of modification of the perovskite energy level by adsorbed benzenethiols. Nevertheless, analysis undertaken on different samples and at different spots provided satisfactorily consistent results that are summarised below. Specifically, modification with HS-Ph-CN and HS-Ph-NO_2 up-shifted E_{vb} of the perovskite to approximately -5.6 eV, while an opposite effect and valence band energy of *ca* -5.8 eV was found upon treatment with HS-Ph-SCH_3 and HS-Ph-OCH_3 (**Table S1**). The weakest effect on E_{vb}, though still consistent with the dipole direction, was produced by HS-Ph-F having the lowest dipole moment (μ) among investigated benzenethiols. The observed shifts can be rationalised in terms of the formation of an interfacial dipole moment that can generate a concomitant increase/decrease of the work function and an upward/downward vacuum-level shift at the interface (**Figure 2c**). Further evidence for modulation of the work function in the perovskite surface layer due to modification with HS-Ph-CN was derived from the Kelvin probe

measurements of a contact potential difference ($\Delta\psi$) (**Figure S6**). More negative $\Delta\psi$ obtained for benzenethiol-treated $Cs_{0.05}FA_{0.79}MA_{0.16}PbI_{2.49}Br_{0.51}$ as compared to the intact film further supports a decrease in the work function.

Previous research on colloidal quantum dots (QD) demonstrated that their band energies can be modified by changing the nature of the capping ligand.[41, 42] The identity of the binding functionality and dipole moment of the ligand influence the strength of the QD-ligand surface dipole, thus shifting the valence band maximum (E_{VB}) and conduction band minimum (E_{CB}). For example, E_{VB} of PbS quantum dots treated with 1,2-ethanedithiol (EDT) is up-shifted by 0.2 eV with respect to that of the same QDs modified with tetrabutylammonium iodide. Such EDT treatment creates an electron-blocking/hole-extraction layer on the QD surface and thereby improves both efficiency and stability of the PbS-based solar cells. Moreover, detailed investigations of this system suggested that differences in the Pb-halide and Pb-thiol interactions generate surface dipole moments, which enables favourable band alignment shift at the interface. Based on these results, we hypothesise that the modification of the perovskite surface with HS-Ph-CN can also change the interfacial dipole moment and band alignment and thereby facilitate charge-transfer (**Figure 2c**).

To investigate the effects of interfacial benzenethiol on the charge transfer between perovskite and HTM, photoluminence (PL) measurements were undertaken. All examined films displayed qualitatively similar PL spectra with a maximum at around 770 nm, and stronger quenching was always observed for the benzenethiol-treated samples (**Figure 3a**). We have further analysed the charge transfer kinetics through the time-resolved photoluminescence (TRPL) measurements (**Figure 3b**). The PL decay curves were fitted using a bi-exponential dependence, where the fast process is caused by bimolecular recombination of photo-generated free carriers, and slow decay process is attributed mainly to trap-assisted recombination (**Table S2**).[43] Unmodified perovskite|HTM sample exhibited an average PL lifetime of 68 ns, which was notably shortened upon interfacial modification with benzenethiols down to 53 (HS-Ph-CN), 15 (HS-Ph-NO_2), 29 (HS-Ph-SCH_3) and 22 ns (HS-Ph-OCH_3). These results suggest that the benzenethiol molecules facilitate faster charge transfer between the perovskite and HTM, which is beneficial to the hole extraction process and therefore better device performance can be expected. Thus, our PL results are in line with the previous work on EDT-treated PbS quantum dots mentioned above,[41] as well as with the reports on improvement of charge-transfer at the perovskite|HTM interface provided by the formation of Pb-S coordination bonds.[44, 45] Importantly, additional washing of the modified perovskite films with chlorobenzene induced marginal changes in the steady-state photoluminescence spectra, attesting to the firm immobilisation of the examined benzenethiols on the $Cs_{0.05}FA_{0.79}MA_{0.16}PbI_{2.49}Br_{0.51}$ surface (**Figure S7**).

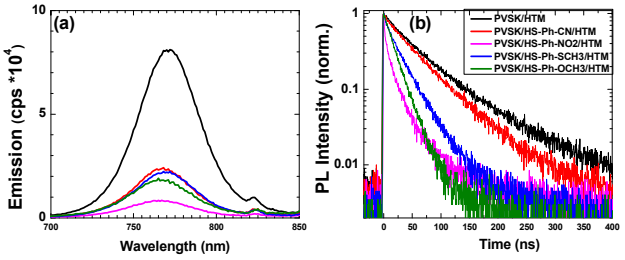

Figure 3. Effects of benzenethiols on the photoluminescence properties of $Cs_{0.05}FA_{0.79}MA_{0.16}PbI_{2.49}Br_{0.51}$: (a) steady-state PL spectra, (b) time-resolved PL decay curves. The perovskite layer was either unmodified, or treated with HS-Ph-CN, HS-Ph-NO_2, HS-Ph-SCH_3, or HS-Ph-OCH_3. Excitation wavelength was 465.8 nm in all experiments.

To further investigate the charge transfer between the perovskite and benzenethiol molecules, PL and TRPL measurements were carried out with no HTM present. Again, modification of $Cs_{0.05}FA_{0.79}MA_{0.16}PbI_{2.49}Br_{0.51}$ induced quenching of the PL intensity by 80-95 % (**Figure S8**) and lifetime from 7.6 to 0.5-1.2 µs (**Table S2**). Thus, both steady-state PL and TRPL results support our hypothesis on the charge transfer from perovskite to benzenethiols. Indeed, this transfer is energetically favourable, as the HOMO levels of all examined benzenethiol molecules inferred from the photoelectron spectroscopy in air (PESA) analysis (**Figure S9**) are more positive than the valence band edge of the perovskite. It can be further suggested that the detected hole trapping can be due to a redox transformation of a benzenethiol that corresponds to an energy level situated higher than E_{VB} of the perovskite (**Figure 2c**). In this case, trapped holes in thiol molecules would produce thyil radicals, which can undergo bimolecular recombination with the formation of disulphide species.[46] When HTM is present, it can directly accept trapped holes from the benzenethiol molecules. Thus, we suggest that the benzenethiol molecules between perovskite and HTM function as a hole extraction interlayer, which can facilitate the charge-extraction process in a working device.

Photovoltaic performance

All photovoltaic measurements were undertaken under simulated 1 sun illumination (100 mW cm^{-2} intensity, AM 1.5 G spectrum). In the initial tests aimed to explore the effects of different benzenethiol molecules on the performance of FTO|c-TiO_2|m-TiO_2 + $Cs_{0.05}FA_{0.79}MA_{0.16}PbI_{2.49}Br_{0.51}$|spiro-OMeTAD|Au solar cells (cross section SEM images are shown in **Figure S10**), photocurrent density (*J*) *vs.* voltage (*V*) characteristics and incident photon-to-charge carrier efficiency (IPCE) spectra were recorded with a small aperture providing an irradiated area of 0.16 cm^2 (**Figure S11**). Major photovoltaic parameters derived from these data are summarised in **Table 1**. The set of unmodified devices with no interfacial modification showed comparatively high and well-reproducible performance.[36] The best solar cell of this type examined here exhibited an open circuit voltage (V_{OC}) of 1.08 V, short circuit current density (J_{SC}) of 22.7 mA cm^{-2}, a fill factor (FF) of 0.78 and a PCE of 19.0%.

Table 1. Effect of benzenethiol interfacial modification on the photovoltaic parameters[a] of the FTO|c-TiO_2|m-TiO_2 + $Cs_{0.05}FA_{0.79}MA_{0.16}PbI_{2.49}Br_{0.51}$|spiro-OMeTAD|Au solar cells with a 0.16 cm^2 aperture.

Device		V_{OC} (mV)	J_{SC} (mA cm^{-2})	FF	PCE (%)	SPO[b] (%)
unmodified	Best	1076	22.7 (21.0)	0.78	19.0 (17.6)	18.4
	Average	1081 ± 9	22.2 ± 0.1	0.77 ± 0.02	18.4 ± 0.4	
HS-Ph-CN	Best	1106	22.8 (21.3)	0.80	20.2 (18.8)	19.6
	Average	1102 ± 22	22.4 ± 0.6	0.78 ± 0.03	19.1 ± 0.7	
HS-Ph-NO_2	Best	1108	22.9 (21.0)	0.79	20.0 (18.4)	19.3
	Average	1097 ± 10	22.4 ± 0.3	0.78 ± 0.01	19.1 ± 0.2	
HS-Ph-SCH_3	Best	1090	22.2 (20.8)	0.79	19.1 (17.9)	18.5
	Average	1088 ± 11	21.9 ± 0.3	0.78 ± 0.01	18.6 ± 0.3	
HS-Ph-OCH_3	Best	1087	22.7 (20.7)	0.78	19.4 (17.6)	18.5
	Average	1085 ± 6	22.3 ± 0.40	0.77 ± 0.02	18.8 ± 0.4	

[a] Derived from the *J-V* curves recorded for 25 devices of each type in the forward-bias to short-circuit direction at the scan rate of 0.100 V s^{-1} under 1 sun simulated irradiation; V_{OC} - open-circuit voltage; J_{SC} – short-circuit current density (values in brackets were obtained *via* integration of the IPCE spectra; see discussions in the text explaining the differences between J_{SC} derived from the *J-V* and IPCE data); FF – fill factor; PCE – power conversion efficiency (values in brackets were calculated using J_{sc} derived from the IPCE spectra). [b] Steady-state power conversion efficiency measured for the best-performing device at the potential corresponding to the maximum power point in the *J-V* curve.

Treatment of the perovskite surface with benzenethiols prior to deposition of a HTM layer produced solar cells that deliver photocurrent densities and FFs like those for unmodified devices, but their V_{OC} was increased by *ca* 5-20 mV (**Table 1**). Reproducibility of this improvement attests to the reliability of the effect. Inspection of the data in **Table 1** and **Table S1** suggests that HS-Ph-CN and HS-Ph-NO_2 benzenethiols having their dipole moments pointing away from the perovskite surface and thereby inducing a positive shift of the valence band edge of the light-absorber (**Figure 2c**) provide higher improvements in V_{OC} and the photovoltaic efficiency. Conversely, HS-Ph-OCH_3 and HS-Ph-SCH_3 having dipole moments oriented in the opposite direction induce negative shift of E_{vb} (**Figure 2c**) and increase the open-circuit voltage to a smaller extent (**Table 1**). The fact that methoxy- and methylsulfanyl-substituted benzenethiols also slightly enhance V_{OC} notwithstanding the negative shift of E_{VB} (**Table S1**) can be rationalised in terms of surface trap passivation by the self-assembled monolayers of these compounds on the perovskite surface.[47] Importantly, control experiments where the perovskite surface was pre-treated with either pure chlorobenzene or HS-free anisole (chlorobenzene solution) produced essentially no improvements in V_{OC} and other photovoltaic parameters (**Figure S12**).

Thus, the use of HS-Ph-CN to modify the perovskite surface produced the highest efficiencies, among which the best result corresponds to the following set of parameters: V_{OC} = 1.11 V, J_{SC} = 22.8 mA cm^{-2}, FF = 0.80, transient PCE = 20.2% and steady-state PCE = 19.6% at 0.93 V over 500 s (**Figure S13**). The integrated J_{SC} derived from the IPCE spectra are 21.0 and 21.3 mA cm^{-2} for the unmodified and modified devices, respectively, which is lower than the values obtained during the *J-V* measurements (**Table 1**). The following factors contribute to this discrepancy. Our IPCE setup is not sensitive below 350 nm, whereas the solar simulator used for *J-V* measurements produces the full spectrum of real sunlight, which contributes approximately 1 mA cm^{-2} to the difference in J_{sc}. Relationship between J_{SC} and illumination intensity is not strictly linear, which induces further difference of *ca* 1 mA cm^{-2}. Minor difference of 0.5 mA cm^{-2} is attributed to the experimental uncertainties.

Further, PSCs having an active area of more than 1.4 cm^2 (aperture area 1.00 cm^2) with or without a HS-PH-CN interfacial layer were fabricated and tested (**Figure 4a** and **Table 2**). The unmodified devices (no benzenethiol interlayer) showed the best performance with V_{OC} of 1.10 V, J_{SC} of 23.2 mA cm^{-2}, FF of 0.71 and PCE of 18.5%, which compares well with previously reported results.[30] Notable improvement in all photovoltaic parameters was achieved *via* modification of the perovskite with HS-PH-CN, which provided the devices with the characteristics as high as V_{OC} = 1.11 V, J_{SC} = 23.8 mA cm^{-2}, FF = 0.74 and PCE = 19.6%. The increased J_{SC} was due to the improved incident photon-to-current conversion efficiency (IPCE), especially within the wavelength ranges 350-400 nm and 600-700 nm (**Figure 4b**). However, the major contribution to the improved PCE was from the fill factor, which increased from 0.71 to 0.74 (**Table 2**). This improvement can be attributed to the enhanced hole extraction and reduced charge accumulation at the perovskite|HTM interface. During steady state PCE output tracking (conducted by applying a constant bias under continuous AM 1.5G for 4000 s), a drop in the PCE from the unmodified device from 18.5 to 17.2% was observed, whereas the HS-PH-CN-modified solar cell exhibited a more robust behaviour with efficiency only slightly decreasing from 19.4 to 19.0% (**Figure 4c**). This PCE decrease is attributed mainly to a continuous heating of the working devices, as no cooling was provided during the measurements. This observation indicates an improved stability provided by the interfacial modification with benzenethiols, which is discussed in more detail in the next sub-section.

Importantly, the devices displayed excellent reproducibility as concluded from testing 20 solar cells in five independent batches with and without benzenethiol modification (**Figure 4d**). Moreover, *J-V* curves measured for five non-overlapping regions at the centre and corners of the large device using an aperture of 0.16 cm^2 also demonstrated very consistent set of photovoltaic parameters, which indicates homogeneous distribution of the cell components over the square-centimetre scale area (**Figure S14**, **Table S4**). Electroluminescence imaging technique[48] also confirmed the uniformity of the perovskite and charge-transfer layers in the

active area of the unmodified and HS-Ph-CN-modified devices (**Figure S15**).

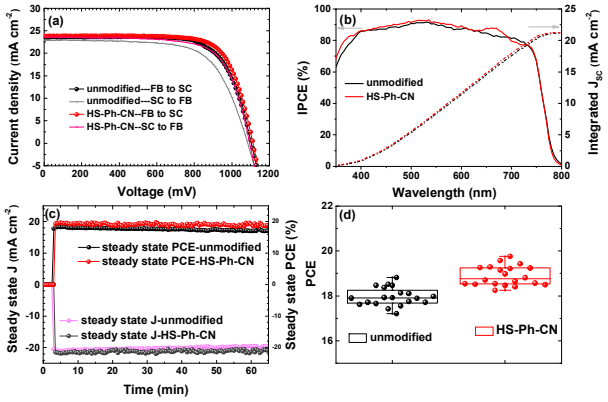

Figure 4. Photovoltaic performance of the large area (aperture 1.00 cm^2) $Cs_{0.05}FA_{0.79}MA_{0.16}PbI_{2.49}Br_{0.51}$-based solar cells without (*black* and *grey*) and with interfacial HS-Ph-CN modification (*red* and *magenta*): (a) *J vs. V* curves (scan rate 100 mV s^{-1}) recorded in the forward bias (FB) to short-circuit (SC), and SC to FB directions; (b) IPCE spectra. Surface of the perovskite layer was either unmodified (*black*), or treated with HS-Ph-CN (*red*); (c) temporal evolution of photocurrent density and PCE at 0.87 V (unmodified) and 0.90 V (treated with HS-Ph-CN); (d) reproducibility of major photovoltaic parameters within 20 independent devices of each type. All measurements under AM 1.5G 1 sun irradiation.

Table 2. Photovoltaic parameters of the larger area (aperture 1.00 cm^2) FTO|c-TiO_2|m-TiO_2 + $Cs_{0.05}FA_{0.79}MA_{0.16}PbI_{2.49}Br_{0.51}$|spiro-OMeTAD|Au devices with and without HS-Ph-CN interfacial treatment under AM 1.5G 1-sun simulated irradiation.[a]

Device			V_{OC} (mV)	J_{SC} (mA cm^{-2})	FF	PCE (%)
unmodified	average FB to SC[b]		1096 ± 16	23.2 ± 0.5	0.71 ± 0.02	18.0 ± 0.4
	best	SC to FB	1085	22.9	0.67	16.6
		FB to SC	1104	23.6	0.71	18.5
HS-Ph-CN	average FB to SC[b]		1116 ± 10	23.5 ±0.5	0.72 ± 0.02	18.9 ± 0.4
	best	SC to FB	1095	23.7	0.70	18.3
		FB to SC	1113	23.9	0.74	19.6

[a] Derived from the *J-V* curves recorded for 20 devices of each type in the forward-bias to short-circuit direction at the scan rate of 0.100 V s^{-1} under 1 sun simulated irradiation; V_{OC} - open-circuit voltage; J_{SC} – short-circuit current density; FF – fill factor; PCE – power conversion efficiency. [b] Steady-state power conversion efficiency measured for the best-performing device at the potential corresponding to the maximum power point in the *J-V* curve.

To obtain deeper insights into the impact of benzenethiol modification on charge-carrier dynamics and enhanced performance of the PSCs, the influence of light intensity (P) on J_{SC} and V_{OC} characteristics was investigated. Analysis of the obtained J_{SC} *vs. P* data in bilogarithmic coordinates revealed that the photocurrent density depends linearly on the irradiation intensity for both unmodified and HS-Ph-CN-treated devices (**Figure 5a**). According to the literature, this indicates that the solar cells examined herein are not significantly affected by the space charge effect.[49, 50] High quality of the devices was further confirmed by linear dependence of the V_{OC} on logarithm of light intensity (**Figure 5b**). This is consistent with the fundamental relationship $V_{OC} = n\ k_BT/q\ln(P)$, where n is a constant often referred to as *ideality factor*, k is Boltzmann's constant, T is temperature and q is the elementary charge. Properties of a solar cell at open circuit are strongly dependent on the recombination processes, since there is no current extraction under these conditions and all photo-generated charge carriers recombine. According to a previous study,[51] the light-intensity dependence of V_{OC} can provide insights into the role of trap-assisted recombination *versus* bimolecular recombination at open-circuit. It is generally accepted that the *ideality factor* should be equal to 1 if Langevin recombination dominates, whereas additional involvement of the interfacial trap-assisted Shockley–Read–Hall (SRH) recombination would result in n greater than 1.[52] The ideality factors obtained for unmodified (1.73) and HS-PH-CN-modified (1.64) devices imply that trap-assisted SRH recombination is present in both devices. The values of n measured here for $Cs_{0.05}FA_{0.79}MA_{0.16}PbI_{2.49}Br_{0.51}$-based PSCs are consistent with the literature reports on triple cation analogues.[53, 54] Smaller n provided by the HS-PH-CN treatment also suggests that the benzenethiol molecules suppress the SRH recombination and consequently lead to the improvement of the photovoltaic performance.

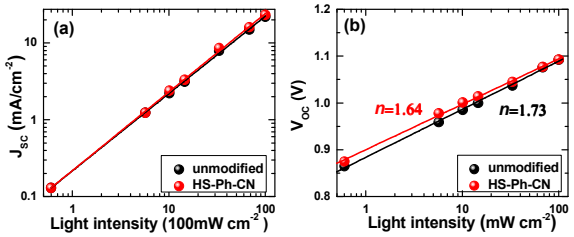

Figure 5. Dependence of (a) J_{SC} and (b) V_{OC} of unmodified (*black*) and HS-Ph-CN-treated (*red*) $Cs_{0.05}FA_{0.79}MA_{0.16}PbI_{2.49}Br_{0.51}$-based solar cells (aperture 1.00 cm^2) on the light intensity. Lines show linear fits to the experimental data.

To further examine the effects of interfacial HS-Ph-CN modification on recombination and charge-extraction in PSCs, the transient photovoltage decays (TVD) and transient photocurrent decays (TCD) at modulated light intensity were measured. The TVD data could be well-fitted with a bi-exponential function, which indicates the presence of two distinct populations of the photogenerated carriers that recombine independently.[55] Corresponding lifetimes, τ_1 and τ_2, were within the range 0.2-10 μs and 50–200 μs, respectively. According to previous report,[55] the charge population with a longer lifetime (τ_2) is associated with electrons transported through the TiO_2 matrix to the FTO anode, while the faster decaying component (τ_1) is due to the charges confined within a perovskite layer and recombining with holes in HTM. Indeed, the τ_2 values within the relevant V_{OC} range for unmodified and HS-Ph-CN-treated devices were very similar (**Figure 6a**), as expected for solar cells featuring identically prepared FTO|TiO_2 components. However, a clear difference in the τ_1-V_{OC} profiles due to the benzenethiol modification was found, which was especially pronounced at higher light intensities (**Figure 6a**). Importantly, this faster process occurring at the perovskite|HTM boundary was the predominant charge

recombination pathway in the solar cells examined here, as concluded on the basis of the fitting amplitude values (**Table S4**). The latter observation is also consistent with previous studies.[55] The transient photocurrent decay data were fitted with exponential dependence to derive the charge-extraction times, which were always faster for the HS-Ph-CN-based devices (**Figure 6b**). This result indicates that the benzenethiol treatment reduces the concentration of charge traps and allows for more efficient charge extraction.

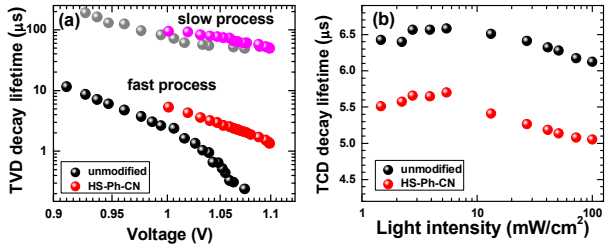

Figure 6. (a) Recombination lifetime *versus* the open-circuit voltage (derived from transient photovoltage decays at modulated light intensity), and (b) extraction lifetime *versus* light intensity (derived from transient photocurrent decays at modulated light intensity) for unmodified and HS-Ph-CN-treated $Cs_{0.05}FA_{0.79}MA_{0.16}PbI_{2.49}Br_{0.51}$-based solar cells.

Taken together, the above TVD and TCD observations along with the PL and UPS data suggest that the conduction band offset between perovskite+HS-Ph-CN and HTM can provide a barrier that prevents photogenerated electrons from flowing to the hole transporter, whereas the valence band bending can intensify the flow of photogenerated holes to the spiro-OMeTAD layer. Thus, the presented experimental evidence indicates that the HS-Ph-CN modification of the perovskite produces an interfacial hole extracting/electron-blocking layer, which reduces the charge recombination and facilitates the transfer of holes from light-harvester into the hole transport material.[39] This can explain the improvements in V_{OC} and FF of the HS-Ph-CN-modified devices (**Figure 4**).

Device stability and long-term performance

Degradation of the $Cs_{0.05}FA_{0.79}MA_{0.16}PbI_{2.49}Br_{0.51}$ films with and without benzenethiol surface modification that were directly exposed to ambient conditions (air, 45 ± 10% relative humidity, 22 ± 2 °C, and continuous ambient room lighting) was monitored for 66 days. During these experiments, the unmodified perovskite film completely decomposed to PbI_2, as inferred from the evolution of sharp peak at 12.6° and disappearance of the perovskite peak at 14.1° in XRD patterns (**Figure S16a**). Improvement in the film stability, *viz.* slower evolution of the PbI_2 diffraction signals, was provided by treatment of the perovskite with HS-Ph-NO_2 and HS-Ph-CN (**Figure S16b and c**), but not with HS-Ph-OCH_3 and HC-Ph-SCH_3 (**Figure S16d and e**). Interestingly, the former two molecules exhibit a dipole moment pointing away from the perovskite, while the methoxy- and methylsulfanyl-substituted benzenethiols have dipole moments pointing towards the $Cs_{0.05}FA_{0.79}MA_{0.16}PbI_{2.49}Br_{0.51}$ film. The underlying reasons for the observed phenomenon are yet to be established.

Further stability tests were undertaken with 1 cm^2 devices. The performance of the non-encapsulated HS-Ph-CN-modified solar cells stored at 22 °C under dark on air with <30% relative humidity was tracked for 264 days. The devices retained 90% of the initial performance after this long-term storage test (**Figure 7ai-di** and **Figure S17)**.

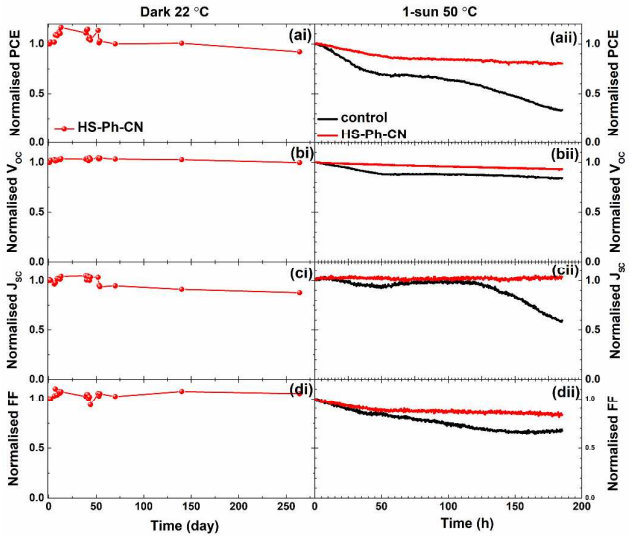

Figure 7. Evolution of normalised (a) PCE, (b) V_{OC}, (c) J_{SC} and (d) FF for (i) non-encapsulated HS-Ph-CN-treated $Cs_{0.05}FA_{0.79}MA_{0.16}PbI_{2.49}Br_{0.51}$-based PSCs (aperture 1.00 cm^2) stored at 22°C under dark in a dry-box (RH < 30%), and (ii) encapsulated $Cs_{0.05}FA_{0.79}MA_{0.16}PbI_{2.49}Br_{0.51}$-based PSCs (aperture 1.00 cm^2) without (*black*) and with (*red*) interfacial HS-Ph-CN modification under 1 sun AM 1.5G irradiation at 50°C (device temperature) in air at a relative humidity of 50%. Data were extracted from SC to FB sweeps of *J-V* curves recorded at 100 mV s^{-1}. Starting parameter values were: (i) PCE = 17.0%, J_{SC} = 22.8 mA cm^{-2}, V_{OC} = 1.09 V, FF = 0.69; (ii) PCE = 17.9 and 19.2%, V_{OC} = 1.09 and 1.13 V, J_{SC} = 22.8 and 23.6 mA cm^{-2}, FF = 0.72 and 0.72 for the unmodified and HS-Ph-CN-modified devices, respectively.

The stability of encapsulated PSCs was studied under continuous simulated 1 sun AM1.5G light soaking in an environmental chamber at a constant relative humidity of 50 % and temperature of 50 °C. These conditions were chosen to mimic the real working environment of solar cells. Juxtaposition of the evolution of normalised PCE, J_{SC}, V_{OC} and FF for the unmodified and HS-Ph-CN-modified devices demonstrates significant improvements in robustness provided by this benzenethiol interfacial layer (**Figure 7aii-dii**). Indeed, PCE of the benzenethiol-free solar cell degraded from 18.0% down to 6.1% over 185 hours of test, in keeping with previous reports.[57] Conversely, the performance of the HS-Ph-CN-modified devices decreased from 19.2 to 16.2% after initial 50 h and then suffered very small degradation during subsequent 135 h of the experiment (**Figure 7aii**). Remarkably, only minor deterioration in V_{OC} was observed (**Figure 7bii**) and J_{SC} did not undergo any changes (**Figure 7cii**) in this experiment, which further confirms the capacity of HS-Ph-CN to stabilise $Cs_{0.05}FA_{0.79}MA_{0.16}PbI_{2.49}Br_{0.51}$ perovskite. Major losses in the efficiency of the PSCs with interfacial benzenethiol modification were due to degradation of the fill factor, which however, was much more pronounced for unmodified devices (**Figure 7dii**). This positive effect of the HS-

Ph-CN modification on FF might be associated with the suppression of the corrosion reaction between inherent ionic defects in the perovskite layer and gold species migrated from the anode.[58] The overall improvement in the stability of PSCs is rationalised in terms of suppressed interfacial recombination provided by the HS-Ph-CN interlayer.

Finally, device stability was additionally assessed at 60 °C, which is expected to induce phase transition in the perovskite[59] These tests were undertaken in the dark and under continuous 1 sun irradiation. In both cases, evident stability improvement after the HS-Ph-CN treatment was observed (**Figures S18** and **S19**). However, significant deterioration in the performance of the 1 cm^2 encapsulated HS-Ph-CN-modified solar cells was observed after 100 h under light and 380 h in the dark at 60 °C.

Based on above results, we hypothesise that the stability improvement provided by the HS-Ph-CN modification is majorly due to the reduced charge accumulation[60] rather than intrinsic stabilisation of the perovskite phase. Indeed, the latter effect can be hardly expected given that the benzenethiol molecules are confined to the perovskite|HTM interface and do not penetrate into the bulk of the light-absorber. Overall, the improvements in the stability found here compare well to the results reported in recent studies focused on creation of more robust PSCs (**Table S5**).

Conclusions

In summary, we developed a facile strategy to improve the power conversion efficiency and substantially enhance the stability of perovskite solar cells *via* modification of the interface between light-harvester and hole transporting layers with benzenethiol dipoles. Synchrotron X-ray photoelectron spectroscopy confirms immobilisation of the benzenethiol molecules on the perovskite film surface. Such modification facilitates hole extraction from perovskite to HTM and suppresses recombination of electrons from the perovskite layer with holes from hole-transporter, as concluded from the photoluminescence and transient photocurrent/photovoltage decay data. The highest power conversion efficiency of 20.2% for the small area devices (0.16 cm^2) and 19.6% for the PSCs with an active area over 1 cm^2 under 1 sun AM 1.5G irradiation was achieved with solar cells modified with HS-Ph-CN. Under simulated solar cell working conditions (1 sun AM 1.5G irradiation, 50% RH, 50 °C device temperature), such devices retained more than 80% of their initial photovoltaic performance after 50 h and operated stably over the next 135 h. In contrast, unmodified PSCs suffered continuous degradation and retained only 35% of their initial PCE after 185 h of tests. The results reported herein emphasise the critical importance of interfacial layer at the perovskite|HTM for high efficiency and especially stability of larger-area perovskite solar cells and offer an efficient method for fabrication of better performing devices of this type.

Conflicts of interest

There are no conflicts to declare.

Acknowledgements

The authors acknowledge the Australian Centre for Advanced Photovoltaics (ACAP), the Australian Renewable Energy Agency and the ARC Centres of Excellence in Exciton Science (ACEX; CE170100026) and in Electromaterials Science (ACES; CE140100012). The authors acknowledge the use of facilities within the Monash University Centre for Electron Microscopy (MCEM) and Monash X-ray Platform (funded by Australian Research Council grant LE130100072).

References

1. M. A. Green and S. P. Bremner, *Nat. Mater.*, 2017, **16**, 23.
2. M. A. Green, *Nat. Energy*, 2016, **1**, 15015.
3. W. S. Yang, B.-W. Park, E. H. Jung, N. J. Jeon, Y. C. Kim, D. U. Lee, S. S. Shin, J. Seo, E. K. Kim and J. H. Noh, *Science*, 2017, **356**, 1376.
4. D. P. McMeekin, G. Sadoughi, W. Rehman, G. E. Eperon, M. Saliba, M. T. Hörantner, A. Haghighirad, N. Sakai, L. Korte and B. Rech, *Science*, 2016, **351**, 151.
5. M. Saliba, T. Matsui, K. Domanski, J.-Y. Seo, A. Ummadisingu, S. M. Zakeeruddin, J.-P. Correa-Baena, W. R. Tress, A. Abate and A. Hagfeldt, *Science*, 2016, **354**, 206.
6. J. Lu, L. Jiang, W. Li, F. Li, N. K. Pai, A. D. Scully, C. M. Tsai, U. Bach, A. N. Simonov and Y. B. Cheng, *Adv. Energy Mater.*, 2017, **7**, 1700444.
7. M. Xiao, F. Huang, W. Huang, Y. Dkhissi, Y. Zhu, J. Etheridge, A. Gray-Weale, U. Bach, Y. B. Cheng and L. Spiccia, *Angew. Chem. Int. Ed.*, 2014, **126**, 10056.
8. F. Huang, Y. Dkhissi, W. Huang, M. Xiao, I. Benesperi, S. Rubanov, Y. Zhu, X. Lin, L. Jiang and Y. Zhou, A. Gray-Weale, J. Etheridge, C. McNeill, R. Caruso, U. Bach, L. Spiccia, Y. B. Cheng, *Nano Energy*, 2014, **10**, 10.
9. F. Huang, A. R. Pascoe, W. Q. Wu, Z. Ku, Y. Peng, J. Zhong, R. A. Caruso and Y. B. Cheng, *Adv. Mater.*, 2017, **29**, 1601715.
10. W. Wu, F. Huang, D. Chen, Y. B. Cheng and R. A. Caruso, *Adv. Energy Mater.*, 2016, **6**, 1502027.
11. T. Qin, W. Huang, J.-E. Kim, D. Vak, C. Forsyth, C. R. McNeill and Y.-B. Cheng, *Nano Energy*, 2017, **31**, 210.
12. H. Kim, K.-G. Lim and T.-W. Lee, *Energy Environ. Sci.*, 2016, **9**, 12.
13. A. Fakharuddin, L. Schmidt-Mende, G. Garcia-Belmonte, R. Jose and I. Mora-Sero, *Adv. Energy Mater.*, 2017, **7**, 1700623.
14. A.-N. Cho and N.-G. Park, *ChemSusChem*, 2017, **10**, 3687.
15. M. Grätzel, *Acc. Chem. Res.*, 2017, **50**, 487.
16. L. M. Herz, *ACS Energy Lett.*, 2017, **2**, 1539.
17. N. K. Noel, A. Abate, S. D. Stranks, E. S. Parrott, V. M. Burlakov, A. Goriely and H. J. Snaith, *ACS Nano*, 2014, **8**, 9815.
18. N. Ahn, K. Kwak, M. S. Jang, H. Yoon, B. Y. Lee, J.-K. Lee, P. V. Pikhitsa, J. Byun and M. Choi, *Nat. Commun.*, 2016, **7**, 13422.
19. D. Bryant, N. Aristidou, S. Pont, I. Sanchez-Molina, T. Chotchunangatchaval, S. Wheeler, J. R. Durrant and S. A. Haque, *Energy Environ. Sci.*, 2016, **9**, 1655.
20. T. Leijtens, G. E. Eperon, A. J. Barker, G. Grancini, W. Zhang, J. M. Ball, A. R. S. Kandada, H. J. Snaith and A. Petrozza, *Energy Environ. Sci.*, 2016, **9**, 3472.
21. S. Yang, Y. Wang, P. Liu, Y.-B. Cheng, H. J. Zhao and H. G. Yang, *Nat. Energy*, 2016, **1**, 15016.
22. X. Zheng, B. Chen, J. Dai, Y. Fang, Y. Bai, Y. Lin, H. Wei, X. C. Zeng and J. Huang, *Nat. Energy*, 2017, **2**, 17102.

23. A. Abate, M. Saliba, D. J. Hollman, S. D. Stranks, K. Wojciechowski, R. Avolio, G. Grancini, A. Petrozza and H. J. Snaith, *Nano lett.*, 2014, **14**, 3247.
24. L. Barnea-Nehoshtan, S. Kirmayer, E. Edri, G. Hodes and D. Cahen, *J. Phys. Chem. Lett.*, 2014, **5**, 2408.
25. J. Haruyama, K. Sodeyama, L. Han and Y. Tateyama, *Acc. Chem. Res.*, 2016, **49**, 554.
26. L. Liu, A. Mei, T. Liu, P. Jiang, Y. Sheng, L. Zhang and H. Han, *J. Am. Chem. Soc.*, 2015, **137**, 1790.
27. Y. Lin, L. Shen, J. Dai, Y. Deng, Y. Wu, Y. Bai, X. Zheng, J. Wang, Y. Fang, H. Wei, W. Ma, X. Zeng, X. Zhan and J. Huang, *Adv. Mater.*, 2017, **29**, 1604545.
28. W.-H. Lee, C.-Y. Chen, C.-S. Li, S.-Y. Hsiao, W.-L. Tsai, M.-J. Huang, C.-H. Cheng, C.-I. Wu and H.-W. Lin, *Nano Energy*, 2017, **38**, 66.
29. W. Chen, Y. Wu, Y. Yue, J. Liu, W. Zhang, X. Yang, H. Chen, E. Bi, I. Ashraful and M. Grätzel, *Science*, 2015, **350**, 944.
30. X. Li, D. Bi, C. Yi, J.-D. Décoppet, J. Luo, S. M. Zakeeruddin, A. Hagfeldt and M. Grätzel, *Science*, 2016, **353**, 58.
31. H. Chen, F. Ye, W. Tang, J. He, M. Yin, Y. Wang, F. Xie, E. Bi, X. Yang M. Grätzel and L. Han, *Nature*, 2017, **550**, 92.
32. L. K. Ono, N.-G. Park, K. Zhu, W. Huang and Y. Qi, *ACS Energy Lett.*, 2017, **2**, 1749.
33. E. Bi, H. Chen, F. Xie, Y. Wu, W. Chen, Y. Su, A. Islam, M. Grätzel, X. Yang and L. Han, *Nat. Commun.*, 2017, **8**, 15330.
34. W. Qiu, T. Merckx, M. Jaysankar, C. M. de la Huerta, L. Rakocevic, W. Zhang, U. Paetzold, R. Gehlhaar, L. Froyen and J. Poortmans, *Energy Environ. Sci.*, 2016, **9**, 484.
35. C.-H. Chiang, M. K. Nazeeruddin, M. Grätzel and C.-G. Wu, *Energy Environ. Sci.*, 2017, **10**, 808.
36. M. Saliba, T. Matsui, J.-Y. Seo, K. Domanski, J.-P. Correa-Baena, M. K. Nazeeruddin, S. M. Zakeeruddin, W. Tress, A. Abate and A. Hagfeldt, *Energy Environ. Sci.*, 2016, **9**, 1989.
37. M. Shalom, S. Ruhle, I. Hod, S. Yahav and A. Zaban, *J. Am. Chem. Soc.*, 2009, **131**, 9876.
38. B. C. C. Cowie, A. Tadich and L. Thomsen, *AIP Conf. Proc.*, 2010, **1234**, 307.
39. Y. Cao, A. Stavrinadis, T. Lasanta, D. So and G. Konstantatos, *Nat. Energy*, 2016, **1**, 16035.
40. B. Philippe, M. Saliba, J.-P. Correa-Baena, U. B. Cappel, S.-H. Turren-Cruz, M. Grätzel, A. Hagfeldt and H. Rensmo, *Chem. Mater*, 2017, **29**, 3589.
41. C.-H. M. Chuang, P. R. Brown, V. Bulović and M. G. Bawendi, *Nat. Mater.*, 2014, **13**, 796.
42. P. R. Brown, D. Kim, R. R. Lunt, N. Zhao, M. G. Bawendi, J. C. Grossman and V. Bulović, *ACS Nano*, 2014, **8**, 5863.
43. D. Bi, W. Tress, M. I. Dar, P. Gao, J. Luo, C. Renevier, K. Schenk, A. Abate, F. Giordano and J.-P. C. Baena, *Sci. Adv.*, 2016, **2**, e1501170.
44. J. Cao, J. Yin, S. Yuan, Y. Zhao, J. Li and N. Zheng, *Nanoscale*, 2015, **7**, 9443.
45. J. Cao, Y.-M. Liu, X. Jing, J. Yin, J. Li, B. Xu, Y.-Z. Tan and N. Zheng, *J. Am. Chem. Soc.*, 2015, **137**, 10914.
46. S. F. Wuister, C. de Mello Donega and A. Meijerink, *J. Phys. Chem. B*, 2004, **108**, 17393.
47. L. Zuo, Q. Chen, N. De Marco, Y.-T. Hsieh, H. Chen, P. Sun, S.-Y. Chang, H. Zhao, S. Dong and Y. Yang, *Nano letters*, 2016, **17**, 269-275.
48. A. M. Soufiani, Z. Hameiri, S. Meyer, S. Lim, M. J. Y. Tayebjee, J. S. Yun, A. Ho-Baillie, G. J. Conibeer, L. Spiccia and M. A. Green, *Adv. Energy Mater.*, 2017, **7**, 1602111.
49. C. M. Proctor, C. Kim, D. Neher and T. Q. Nguyen, *Adv. Funct. Mater.*, 2013, **23**, 3584.
50. W. Liao, D. Zhao, Y. Yu, C. R. Grice, C. Wang, A. J. Cimaroli, P. Schulz, W. Meng, K. Zhu and R. G. Xiong, *Adv. Mater.*, 2016, **28**, 9333.
51. M. Mandoc, F. Kooistra, J. Hummelen, B. De Boer and P. Blom, *Appl. Phys. Lett.*, 2007, **91**, 263505.
52. W. Tress, K. Leo and M. Riede, *Appl. Phys. Lett.*, 2013, **102**, 163901.
53. T. Singh and T. Miyasaka, *Adv. Energy Mater.*, 2017, **8**, 1700677.
54. P. Yadav, M. I. Dar, N. Arora, E. A. Alharbi, F. Giordano, S. M. Zakeeruddin and M. Grätzel, *Adv. Mater.*, 2017, **29**, 1701077.
55. B. C. O'Regan, P. R. Barnes, X. Li, C. Law, E. Palomares and J. M. Marin-Beloqui, *J. Am. Chem. Soc.*, 2015, **137**, 5087.
56. V. Roiati, S. Colella, G. Lerario, L. De Marco, A. Rizzo, A. Listorti and G. Gigli, *Energy Environ. Sci.*, 2014, **7**, 1889.
57. J. W. Lee, D. H. Kim, H. S. Kim, S. W. Seo, S. M. Cho and N. G. Park, *Adv. Energy Mater.*, 2015, **5**, 1501310.
58. K. Domanski, J.-P. Correa-Baena, N. Mine, M. K. Nazeeruddin, A. Abate, M. Saliba, W. Tress, A. Hagfeldt and M. Grätzel, *ACS Nano*, 2016, **10**, 6306.
59. A. Alberti, I. Deretzis, G. Mannino, E. Smecca, S. Sanzaro, Y. Numata, T. Miyasaka and A. La Magna, *J. Phys. Chem. C*, 2017, **121**, 13577-13585.
60. N. Aristidou, I. Sanchez‐Molina, T. Chotchuangchutchaval, M. Brown, L. Martinez, T. Rath and S. A. Haque, *Angew. Chem. Int. Ed*, 2015, **54**, 8208-8212

A facile method to produce large metal halide perovskite solar cells with improved stability and efficiency is introduced